Optical characterization of $CuIn_{1-x}Ga_xSe_2$ alloy thin films by spectroscopic ellipsometry

P. D. Paulson, R. W. Birkmire, and W. N. Shafarman[a)]
Institute of Energy Conversion, University of Delaware, Newark, Delaware 19716

(Received 2 January 2003; accepted 18 April 2003)

Optical constants of polycrystalline thin film $CuIn_{1-x}Ga_xSe_2$ alloys with Ga/(Ga+In) ratios from 0 to 1 have been determined by spectroscopic ellipsometry over an energy range of 0.75–4.6 eV. $CuIn_{1-x}Ga_xSe_2$ films were deposited by simultaneous thermal evaporation of elemental copper, indium, gallium and selenium. X-ray diffraction measurements show that the $CuIn_{1-x}Ga_xSe_2$ films are single phase. Due to their high surface roughness, the films are generally not suitable for ellipsometer measurements. A method is presented in which spectroscopic ellipsometer measurements were carried out on the reverse side of the $CuIn_{1-x}Ga_xSe_2$ films immediately after peeling them from Mo-coated soda lime glass substrates. A detailed description of multilayer optical modeling of ellipsometric data, generic to ternary chalcopyrite films, is presented. Accurate values of the refractive index and extinction coefficient were obtained and the effects of varying Ga concentrations on the electronic transitions are presented. © *2003 American Institute of Physics.* [DOI: 10.1063/1.1581345]

I. INTRODUCTION

Polycrystalline $CuIn_{1-x}Ga_xSe_2$ thin films are promising materials for photovoltaic applications. Precise knowledge of the optical properties of these films is an important factor in characterizing and modeling these solar cell devices. There is a significant amount of information available on band structure based on theoretical calculations.[1–3] The $CuIn_{1-x}Ga_xSe_2$ alloy system has been investigated on single or polycrystalline ingots using a spectroscopic ellipsometer (SE).[4–6] However, these studies did not address the possible effects of grain size and polycrystalline texture on the optical properties. SE measurements on $CuIn_{1-x}Ga_xSe_2$ films reported in the literature could not be analyzed due to the high film surface roughness and electronic transitions as a function of the Ga content were not determined.[7,8] Optical transmission, reflection and absorption studies of thin film $CuIn_{1-x}Ga_xSe_2$ have generally been limited to the fundamental absorption edge,[9,10] or did not have sufficient sensitivity to separate the effects of spin–orbit and crystal field interactions near the fundamental band gap. The spin–orbit and crystal field splits have been determined by photoluminescence measurements of $CuIn_{1-x}Ga_xSe_2$ epitaxial films.[11] However, there are no optical data available in the literature for polycrystalline $CuIn_{1-x}Ga_xSe_2$ thin films that show the influence of the Ga content on various electronic transitions over a large spectral range. In this article, the effect of Ga on the optical properties and electronic transitions of $CuIn_{1-x}Ga_xSe_2$ polycrystalline thin films is presented.

In general, it is difficult to model and uniquely determine the optical constants from ellipsometric data on materials with high surface roughness.[7] This article describes a method by which to circumvent the problem associated with the surface roughness by peeling the films from the substrate and performing measurements on the smooth exposed film surface. In addition, a detailed spectroscopic ellipsometer measurement and modeling routine for $CuIn_{1-x}Ga_xSe_2$ polycrystalline thin films is presented. Accurate optical functions for the energy range of 0.75–4.6 eV are presented for films with $x \equiv Ga/(In+Ga)$ from 0 to 1.

II. EXPERIMENTAL DETAILS

A. Deposition and characterization

$CuIn_{1-x}Ga_xSe_2$ films were deposited on Mo-coated soda lime glass substrates by coevaporation from elemental Knudsen type sources for Cu, In, Ga and Se. Elemental fluxes were kept constant throughout the 44 min deposition, giving films with thicknesses of 1.5–2 μm. The substrate temperature was maintained at 550 °C throughout the deposition. Details of the deposition methods can be found elsewhere.[12,13] The compositions of all films were determined by energy dispersive x-ray spectroscopy (EDS) analysis. Depth profiles measured by Auger electron spectroscopy (AES) of selected samples showed that the films had uniform composition through their thicknesses. Atomic force microscopy (AFM) measurements were performed to determine the surface roughness on as-deposited $CuIn_{1-x}Ga_xSe_2$ films and used for the optical modeling. AFM measurements on the peeled $CuIn_{1-x}Ga_xSe_2$ surface were compared with the roughness obtained from the ellipsometer analysis. The structure of the films was characterized by x-ray diffraction (XRD).

B. SE measurement strategy

The AFM measurements showed that the evaporated $CuIn_{1-x}Ga_xSe_2$ films have surface root mean square (rms) roughness on the order of 50–100 nm. It is almost impossible to carry out SE measurements that are useful because

a)Electronic mail: wns@udel.edu

such high surface roughness will not allow the optical functions to be uniquely determined. Mechanical polishing can be used to smooth the films, but it is difficult to ensure that grit is completely removed from the surface and grain boundaries after polishing. Chemical polishing could be another method, but etching may modify the film's surface composition to which SE measurements are highly sensitive. Measurement through the substrate (reverse ellipsometry) is another option, provided the films were deposited on optically transparent (e.g., glass without Mo coating) substrates. However, $CuIn_{1-x}Ga_xSe_2$ deposited on a glass substrate may have different properties than material grown on a glass/Mo substrate. For example, films on a glass substrate were shown to have a much stronger $\langle 112 \rangle$ preferred orientation.[14] Also, with a glass substrate, very thick ($\sim$5 mm) glass is required to prevent front reflection from the glass affecting the measurement.

An alternative way by which to circumvent the surface roughness is to perform the SE measurements on the reverse side of the film after peeling it from the substrate. To prepare a sample, an optically thick (>0.1 μm) Mo film was first deposited on the $CuIn_{1-x}Ga_xSe_2$ film. Then an aluminum substrate was glued to the film using a fast curing epoxy. Because of the optically thick Mo, optical functions of the epoxy are not required for optical modeling. After curing, the Mo/Glass substrate was pulled from the $CuIn_{1-x}Ga_xSe_2$ film, leaving the smooth oxide free back surface of the $CuIn_{1-x}Ga_xSe_2$ film exposed for the SE measurement. In the present configuration, the original rough surface is now on the reverse side, where only higher wavelength probing light can reach. At higher wavelength, the effect of surface roughness is negligible due to reduced scattering. For the transparent region, the ellipsometry data includes contributions from the interface layer and the Mo film. These contributions were modeled with an effective medium layer, described later. In addition, the $CuIn_{1-x}Ga_xSe_2$ films were sufficiently thick so that optical constants in the transparent region could be determined unambiguously. Measurements and fits were carried out at three different incident angles to improve the level of confidence of the fit in the absorbing region.

SE measurements were carried out using a J. A. Woollam company variable angle spectroscopic ellipsometer (VASE). The VASE is a rotating analyzer ellipsometer equipped with an autoretarder, which is useful in measuring the depolarization caused by surface roughness and thickness nonuniformity. Measurements were carried out at room temperature immediately after peeling, with the sample under Ar flow to reduce possible surface contamination. First, VASE scans were done at varying angles to determine the pseudo-Brewster angle of the multilayer structure. For this, scans were performed at two wavelengths (500 and 1500 nm) by varying the angle of incidence from 50° to 85° in 1° steps. The angle corresponding to $\Delta = 90$ and the minimum in ψ provides the pseudo-Brewster angle for that sample.[15] Here Δ and ψ are the ellipsometry parameters that correspond to changes in phase and amplitude induced by the reflection. Then measurements were done at this angle and two additional angles selected by an empirical rule, the pseudo-Brewster angle $\pm 5°$.[16] VASE measurements were carried out between 0.75 and 2 eV in energy steps of 5 meV and between 2 and 4.6 eV with 12.5 meV steps. A small step size in the transparent region was selected specifically to resolve the closely spaced fundamental transitions and the interference fringes. The data acquisition and modeling were performed with the help of WVASE 32™ software supplied by Woollam.

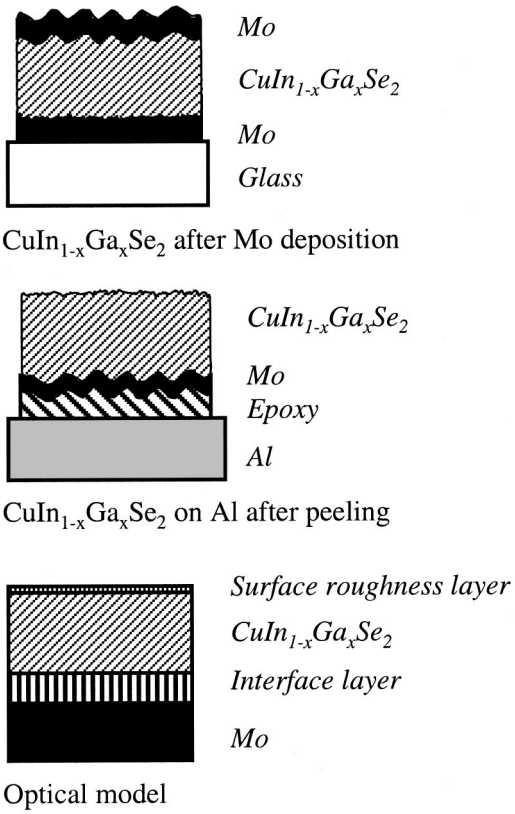

FIG. 1. Sample structure and optical model used for the SE measurement and analysis.

III. OPTICAL MODELING

Chalcopyrite $CuInSe_2$ single crystals exhibit uniaxial anisotropy in their optical properties[17] and display ordinary optical properties (electric field perpendicular to the *c* axis) and extraordinary optical properties (electric field parallel to the *c* axis). For polycrystalline material, the anisotropy is a strong function of the crystallographic texture. If all the crystals have the same texture, the anisotropy of the polycrystalline material would be similar to that of a single crystal. However, if the polycrystalline material has the same probability of occurrence for all textures or is randomly structured the optical properties of the material would be isotropic. The effective dielectric function of the polycrystalline material was calculated as a tensorial average by considering a medium composed of uniaxial crystals oriented in random directions.[18] A Bruggeman effective medium calculation shows that the pseudodielectric function of the randomly oriented polycrystalline material resembles the ordinary component of the single crystal material.[4,19]

Extracting useful information from ellipsometric data begins with the construction of an optical model for the peeled $CuIn_{1-x}Ga_xSe_2$ film on the Mo substrate. Figure 1

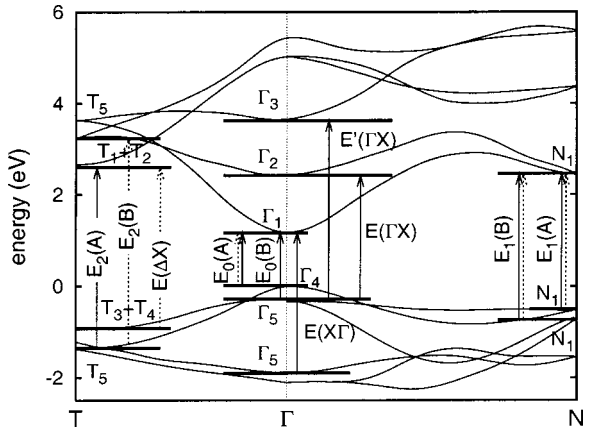

FIG. 2. Generic band structure of a chalcopyrite semiconductor without spin–orbit interaction (from Ref. 6). Dashed and solid arrows represent optical transitions allowed in $E_{\|}c$ and $E_{\perp}c$, respectively.

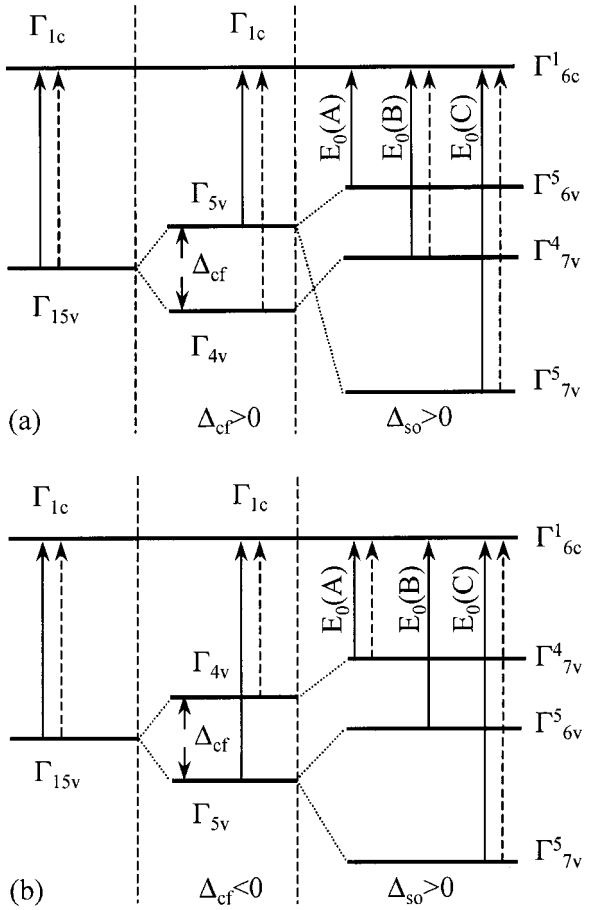

FIG. 3. Schematic diagram showing how the crystal field and spin–orbit interaction leads to formation of nondegenerate energy levels $E_0(A)$, $E_0(B)$ and $E_0(C)$ in (a) $CuInSe_2$ and (b) $CuGaSe_2$ chalcopyrite materials. Dashed and solid arrows represent optical transitions allowed in $E_{\|}c$ and $E_{\perp}c$, respectively. Notation is from Ref. 29.

shows the structure of the $CuIn_{1-x}Ga_xSe_2$ sample and the optical model used for the SE measurement and analysis. The optical model consists of (1) surface roughness on the peeled layer; (2) the $CuIn_{1-x}Ga_xSe_2$ film; (3) an interface layer (the surface layer before peeling); and (4) the Mo layer. It had to be assumed that the optical constants of the Mo film were different from the bulk optical properties. Therefore, the Mo optical constants were obtained from measurements on Mo/$CuIn_{1-x}Ga_xSe_2$ films after depositing the >0.1 μm thick Mo film onto the $CuIn_{1-x}Ga_xSe_2$ and prior to attaching the Al substrate. Optical constants of the Mo layer were then extracted from a two-layer model consisting of a Mo bulk layer and a surface roughness layer, where the surface roughness layer is modeled using a Bruggeman effective medium approximation (EMA) consisting of Mo and a void fraction. Here it is assumed that the surface features are hemispherical in shape and that the corresponding screening parameter is 0.33. Since the Mo film was optically thick, the effect of the $CuIn_{1-x}Ga_xSe_2$ substrate was not considered in this analysis.

The complex dielectric response, $\varepsilon=\varepsilon_1+i\varepsilon_2$, is the manifestation of different interband electronic transitions that result from the electric field applied. The relation between the energy-band structure and ε_2 can be given by[17]

$$\varepsilon_2(E)=\frac{4e^2\hbar^2}{\pi\mu^2E^2}\int dk|P_{cv}(k)|^2\delta[E_c(k)-E_v(k)-E], \tag{1}$$

where μ is the combined density of states (DOS) mass; the Dirac δ function represents the spectral joint DOS between the valance $[E_v(k)]$ and conduction $[E_c(k)]$ band states differing by energy $E=\hbar\omega$ of the incident light; $P_{cv}(k)$ is the momentum-matrix element between the valence and conduction band states; and integration is performed over the first Brillouin zone (BZ). Critical points (CPs) correspond to the energy at which the joint DOS shows strong variations as a function of the energy. In three dimensions, depending on the analytical behavior of the joint DOS, there are four types of CPs, namely, M_0, M_1, M_2 and M_3 present. Figure 2 shows the energy-band diagram for a generic I–III–VI_2 chalcopyrite structure without spin–orbit interaction.[6] The chalcopyrite (CH) band diagram is derived from the zinc blende (ZB) structure because of the similarity in physical properties due to its tetragonal structure.[20]

The valance band maximum at the BZ center is a triply degenerate state. The perturbation due to the tetragonal crystal field resulting from the change in symmetry from ZB to chalcopyrite leads to the nondegenerate states Γ_4 and doubly degenerate Γ_5. Theoretically the crystal field splitting Δ_{cf} can be calculated using the compression formula,[21]

$$\Delta_{cf}=-b\left[1-\frac{c}{2a}\right], \tag{2}$$

where c and a are the lattice constants and b is the deformation potential with a typical magnitude of $\sim$1 eV. Based on this relation the Δ_{cf} changes from positive for $CuInSe_2$ ($c/2a=1.004$) to negative for $CuGaSe_2$ ($c/2a=0.9825$). The doubly degenerate Γ_5 is further split by the spin–orbit interaction.

The fundamental transitions from the valence band maximum to the conduction band minimum at the Γ point are schematically shown in Figs. 3(a) and 3(b). Vertical solid and dashed lines indicate transitions allowed in perpendicular or parallel electric fields, respectively. For a $CuInSe_2$-like CH structure [Fig. 3(a)] Δ_{cf} is positive and Γ_{4v} lies below

TABLE I. EDS data of $Cu(In_{1-x}Ga_x)Se_2$ films used for the SE analysis.

Sample	Cu (%)	In (%)	Ga (%)	Se (%)	Cu/(Ga+In)	Ga/(Ga+In)
A	25.8	25.2	0	49.0	1.02	0.00
B	24.8	18.3	8.3	48.7	0.93	0.31
C	24.0	14.9	12.1	49.0	0.89	0.45
D	24.6	8.9	17.5	48.9	0.93	0.66
E	23.7	0	27.3	49.0	0.87	1.00

Γ_{5v}. For a $CuGaSe_2$-like CH structure [Fig. 3(b)] Δ_{cf} is negative and Γ_{5v} lies below Γ_{4v}. The transitions are conventionally labeled $E_0(A)$, $E_0(B)$ and $E_0(C)$ in order of increasing energy.[4,21,22] The order of the energy levels is determined from the polarization-intensity ratios. The polarization-intensity ratio for the transitions from the Γ_{7v}^4 and Γ_{7v}^5 valence bands to the Γ_{6c}^1 conduction band are given by[21]

$$\frac{I_{\parallel}}{I_{\perp}} = \left[2 - \frac{3\Delta E}{\Delta_{so}}\right]^2, \tag{3}$$

where ΔE is the separation from the totally perpendicularly polarized $\Gamma_{6v}^5 \rightarrow \Gamma_{6c}^1$ transition. The calculated intensity ratios for Γ_{7v}^4, Γ_{7v}^5 and Γ_{6v}^5 transitions in $CuGaSe_2$ crystal are 5:1, 1:4 and 1:1. Experimental determination of these intensity ratios would require measurements on single crystals with the *c* axis perpendicular and parallel to the incident light. In our analysis we used the analogy of single crystal measurements and theoretical calculations to identify the different energy levels.

Experimentally, the transition energies can be obtained from CPs in the ε_2 spectrum of the material, and are best resolved in their numerical second order derivative. The unbiased values of spin–orbit splitting (i.e., spin–orbit splitting in the absence of crystal field splitting) and crystal field splitting (i.e., crystal field splitting in the absence of spin–orbit splitting) were determined using a quasicubic model:[23]

$$\Delta_{so} = \frac{E_1+E_2}{2} + \left[\frac{3}{2}\left(\frac{E_2-E_1}{2}\right)^2 - \frac{1}{2}\left(\frac{E_2+E_1}{2}\right)^2\right]^{1/2}, \tag{4}$$

$$\Delta_{cf} = \frac{E_1+E_2}{2} - \left[\frac{3}{2}\left(\frac{E_2-E_1}{2}\right)^2 - \frac{1}{2}\left(\frac{E_2+E_1}{2}\right)^2\right]^{1/2}, \tag{5}$$

where $E_1 = \Gamma_{7v}^4$ valence band energy $-\Gamma_{6v}^5$ valance band energy and $E_2 = \Gamma_{7v}^5$ valance band energy $-\Gamma_{6v}^5$ valance band energy.

TABLE II. Comparison of the orientation parameter, roughness data from AFM and SE measurements and fit index.

Ga/(Ga+In)	Orientation parameter (P_{hkl})	Roughness from AFM (nm)	Roughness from SE (nm)
0	2.2	5.6	3.5
0.31	1.8	3.7	5.2
0.45	2.7	3.4	6.1
0.66	2.8	14.6	8.8
1.00	2.8	3.1	3.2

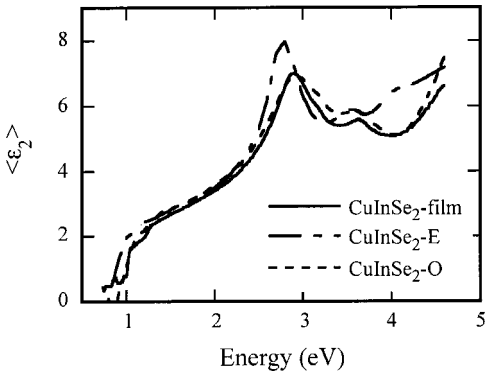

FIG. 4. ε_2 spectrum of the $CuInSe_2$ thin film along with ordinary (O) and extraordinary (E) ε_2 spectra of a $CuInSe_2$ single crystal (from Ref. 6). The film closely matches the ordinary spectrum of the single crystal.

Both the surface and interface layers in the optical model for the peeled film were analyzed with an EMA model. The rms surface roughness measured by AFM of the $CuIn_{1-x}Ga_xSe_2$ film before Mo deposition provided an estimate of the interface layer thickness. The thickness of the $CuIn_{1-x}Ga_xSe_2$ film was obtained by fitting the data in the transparent region of the spectrum using a Cauchy dispersion relation. Then the results for *n* in the transparent region obtained from the Cauchy dispersion relation were used to perform a point-by-point fit starting from the transparent region to extract approximate values of the optical functions. The error in the point-by-point fit, measured by a 90% confidence limit, was determined to check the quality of the *n* and *k* data. The optical functions obtained are called initial spectra and are close to the bulk dielectric response of the bulk film, free of substrate, interface, and surface roughness effects.

The initial spectrum was fit with a general oscillator model which uses linear summation of Kramers–Kronig (KK) consistent oscillators to describe the various optical transitions. The fundamental transitions $E_0(A)$, $E_0(B)$, and $E_0(C)$ in the chalcopyrite crystal have a three-dimensional M_0 CP character.[5] Three parametric Gaussian broadened polynomial superposition (GBPS) semiconductor oscillators[7,24] are used to simulate these transitions. The CPs at higher energies due to transitions at Γ, *N* and *T* points in the BZ were simulated using several harmonic Lorentzian and Gaussian oscillators. The strength, broadening and positions of these oscillators were adjusted to match the initial spectrum. In the next procedure, the expected ellipsometric parameters ψ and Δ of the multilayer structure were generated using this parametric dispersion layer in the optical model. The data generated are compared with the experimental data and fit to reduce the error using the Marquardt–Levenberg algorithm.[25] In this procedure, the thickness and refractive index of the film are slightly adjusted. Also, nonideal features like thickness nonuniformity are introduced into the model to fit the depolarization measured using the autoretarder. The root mean square error (MSE) is used to quantify the difference between experimental and predicted data. The MSE is calculated by

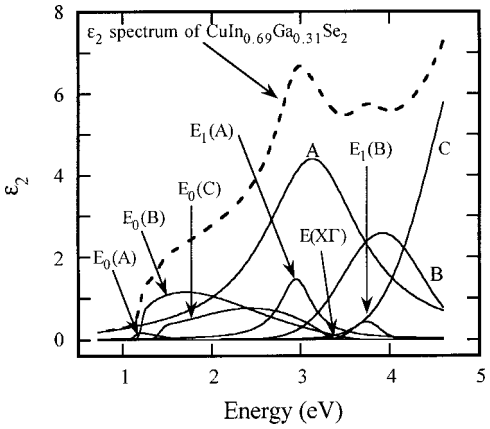

FIG. 5. Initial spectrum (dashed line) of a typical $CuIn_{1-x}Ga_xSe_2$ sample obtained from the point-by-point fit. The spectrum is free of substrate effects as is clear from the absence of interference fringes. Also shown are the different oscillators used to fit the initial spectrum.

$$\mathrm{MSE}=\left\{\frac{1}{2N-M}\sum_{i=1}^{N}\left[\left(\frac{\Psi_i^{\mathrm{mod}}-\Psi_i^{\mathrm{expt}}}{\sigma_{\Psi j}^{\mathrm{expt}}}\right)^2+\left(\frac{\Delta_i^{\mathrm{mod}}-\Delta_i^{\mathrm{expt}}}{\sigma_{\Delta j}^{\mathrm{expt}}}\right)^2\right]\right\}^{1/2}, \tag{6}$$

where $\sigma_{\Psi j,\Delta j}^{\mathrm{expt}}$ is the standard deviation in the measured ellipsometry parameters Ψ and Δ, Ψ_i^{mod} and Δ_i^{mod} are the model generated ellipsometry parameters, Ψ_i^{expt} and Δ_i^{expt} are the measured ellipsometry parameters, N is the number of measured parameters, and M is the number of fitted parameters. By using the experimental standard deviation as the weighting parameter in the fit, the contribution due to noise in the MSE is reduced significantly. The sequence of obtaining the point-by-point fit, adjusting the oscillator strength and then fitting to reduce the MSE, was repeated several times until a minimum value of MSE was obtained without significant parameter correlation. A good fit is obtained when the MSE is close to unity.

IV. RESULTS AND DISCUSSION

$CuIn_{1-x}Ga_xSe_2$ films peeled off of the glass/Mo substrate without significant cracking in the film. EDS measurements on the Mo substrate after removing $CuIn_{1-x}Ga_xSe_2$ show the presence of Se. SE measurements of the Mo substrate indicate the presence of an ~8 nm thick $MoSe_2$ film. This $MoSe_2$ layer weakens the interface between the $CuIn_{1-x}Ga_xSe_2$ film and Mo/glass substrate, allowing clean separation. The peeled $CuIn_{1-x}Ga_xSe_2$ film surface is free of $MoSe_2$ and x-ray photoelectron spectroscopy (XPS) measurement shows that there is no Mo present on the $CuIn_{1-x}Ga_xSe_2$ film.

XRD measurements show that the $CuIn_{1-x}Ga_xSe_2$ films are single phase throughout the whole composition range. Table I shows the composition of all $CuIn_{1-x}Ga_xSe_2$ films used in this work, determined from EDS measurements. The orientation of the crystals with respect to the direction normal to the substrate plane was compared to a random powder orientation using the method of Harris for polycrystalline fiber texture analysis:[26] In this analysis, the orientation parameter P_{hkl} is given by

$$P_{hkl}=n\frac{I_{hkl}}{I_{hkl}^r}\left[\sum_{hkl=1}^{n}\frac{I_{hkl}}{I_{hkl}^r}\right]^{-1}, \tag{7}$$

where I_{hkl} is the intensity of the reflection from the *hkl* plane of the film, I_{hkl}^r is the intensity of the reflection from the *hkl* plane of a reference powder sample with the same phase and n is the number of peaks included in the analysis. The films in this work were all found to have ⟨112⟩ preferred orientation. A film with all the crystals oriented in the ⟨112⟩ direction normal to the substrate plane will have $P_{112}=n$, a film with random grain orientation will have $P_{112}=1$, and a film with grains oriented in a direction other than ⟨112⟩ will have $P_{112}<1$. In this work, five peaks were used for the orientation analysis and the films have orientation parameter P_{112} in the range of 1.8–2.8, as listed in Table II. This indicates that the films are neither randomly nor perfectly oriented.

Figure 4 shows the pseudodielectric function measured for the $CuInSe_2$ film along with the ordinary and extraordinary results for a single crystal reported in the literature.[6] The optical constants of the $CuInSe_2$ film are closer to the ordinary component of the single crystal optical constants. Therefore, the ⟨112⟩ orientation of the films does not cause a measurable change in the optical constants. To confirm this, measurements were performed on these films to determine the off-diagonal elements in the Jones matrix.[27] The data were acquired with the polarizer set at −60°, −30°, 0°, 30° and 60°. These anisotropy measurements showed that the off-diagonal elements were close to zero, confirming that the optical properties are due to the ordinary component. Also, the magnitude of the ε_2 spectrum is similar to that of the single crystal, suggesting that the films are optically dense with insignificant surface roughness and/or an oxide layer. Voids, oxide layers or roughness can reduce the dielectric response of the material and result in a decrease in this ε_2 spectrum.

TABLE III. Oscillator energies corresponding to the electronic transitions with varying Ga/(Ga+In) ratios.

Ga/(Ga+In)	$E_0(A)$ (eV)	$E_0(B)$ (eV)	$E_0(C)$ (eV)	$E_1(A)$ (eV)	$E(X\Gamma)$ (eV)	$E_1(B)$ (eV)	MSE
0.00		1.023	1.247	2.917	3.187	3.662	1.0
0.31	1.168	1.208	1.449	2.965	3.302	3.746	1.7
0.45	1.280	1.351	1.599	3.019	3.345	3.809	1.6
0.66	1.366	1.457	1.641	3.066	3.379	3.917	2.6
1.00	1.689	1.771	1.976	3.168	3.528	4.057	3.0

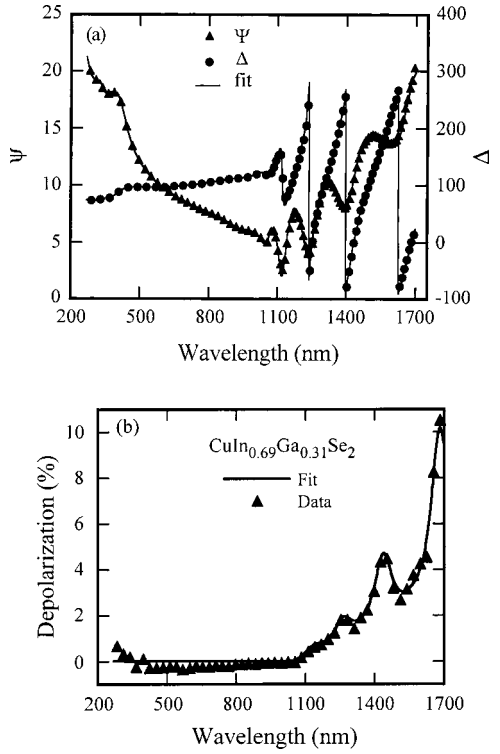

FIG. 6. Measurement and fit of ellipsometry parameters (a) Δ and Ψ and (b) depolarization for the $CuIn_{0.69}Ga_{0.31}Se_2$ film at 70° incident angle. The depolarization is modeled with 3.5% thickness nonuniformity in the $CuIn_{0.69}Ga_{0.31}Se_2$ film.

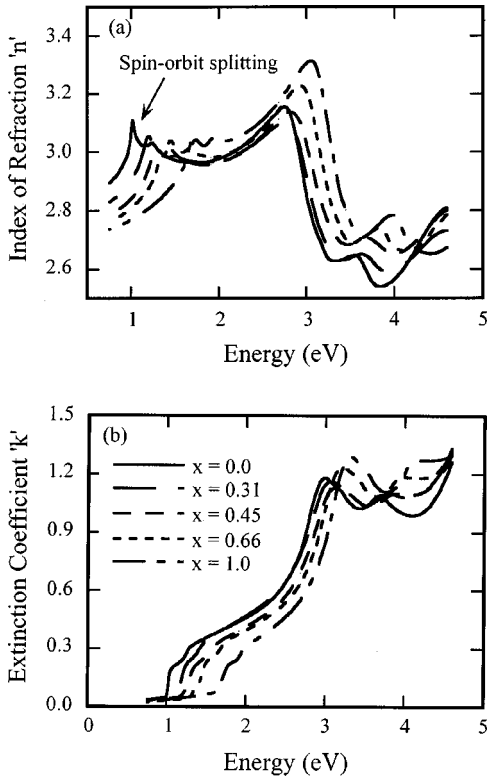

FIG. 8. (a) Index of refraction and (b) extinction coefficient spectra of $CuIn_{1-x}Ga_xSe_2$ films with varying Ga contents. The spin–orbit splitting can be clearly seen.

Optical modeling results in best fits without significant parameter correlation. Figure 5 shows the initial spectrum of a $CuIn_{0.69}Ga_{0.31}Se_2$ film obtained from a point-by-point fit. The 90% confidence limit values were less than 1% of the ε_2 values so the initial spectrum gave a good representation of the bulk optical constants. The spectrum is free of the substrate effect and hence there are no interference fringes. Also shown are the different oscillators used to fit the initial spectrum. In order to fit the initial spectra accurately, more oscillators (labeled *A*, *B*, and *C*) than the number of the CPs in the measurement energy range were used. This was necessitated by residual absorption due to electronic transitions at higher energies, for example, $E_2(A)$, and also to account for possible indirect transitions.[28] The oscillators used in this model provided a good fit for both ε_2 and its derivatives. This approach of generating the initial spectrum and subsequently fitting it with oscillators helps to resolve minor details in ε_2 spectra that cannot be resolved by directly fitting the ellipsometry parameters. Table III lists the oscillator energies that correspond to the electronic transitions in the measurement energy range along with the fit index described in terms of the MSE for all the films. The MSE values are close to unity for low Ga films, indicating the high quality of the fits. The MSE values are slightly higher with higher Ga concentrations due to the increase in the number of interference fringes associated with the shift of the band gap. If we restrict the fit to the absorbing region, the MSE value would be close to unity. Table II also shows a comparison of the surface roughness values obtained from the ellipsometry analysis and rms roughness from AFM measurements. The measurements show the same trend of the roughness variation, although the values are slightly different. This difference may be due to differences in the measurement techniques or to the sample region considered for each measurement. Figure 6(a) shows the measured results and best fit for the ellipsometric parameters Ψ and Δ measured on the $CuIn_{0.69}Ga_{0.31}Se_2$ film at 70° incident angle. The fit was performed at three incident angles, but the data for 65° and 75° incident angles are not shown here for clarity. The *x* axis is shown in terms of wavelength to highlight the fit in the transparent region where the interference fringes dominate the spectrum. Figure 6(b) shows the measurement and fit of the depolarization for the same film at 70° incident angle. The depolarization spectrum

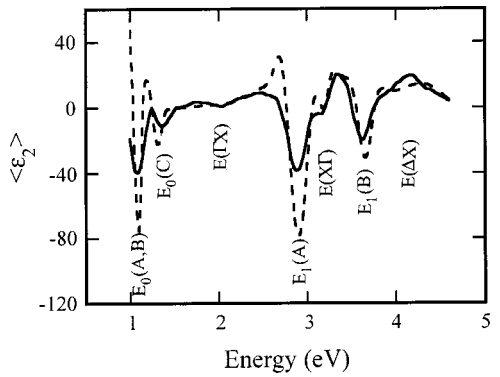

FIG. 7. Second derivatives of the ε_2 spectrum of a $CuInSe_2$ film (solid line) and the ordinary ε_2 spectrum of a $CuInSe_2$ single crystal (dashed line). Critical points correspond to minima in the spectra and are marked.

TABLE IV. Optical constants n and k for $CuInGaSe_2$ with varying x.

E (eV)	$x=0$		$x=0.31$		$x=0.45$		$x=0.66$		$x=1.0$	
	n	k	n	k	n	k	n	k	n	k
4.60	2.81	1.26	2.73	1.33	2.80	1.30	2.78	1.32	2.67	1.30
4.50	2.78	1.16	2.72	1.24	2.78	1.22	2.75	1.26	2.66	1.28
4.40	2.74	1.08	2.70	1.17	2.74	1.16	2.71	1.20	2.65	1.27
4.30	2.69	1.02	2.67	1.12	2.71	1.12	2.68	1.18	2.66	1.27
4.20	2.64	0.99	2.63	1.09	2.68	1.10	2.66	1.18	2.68	1.27
4.10	2.60	0.99	2.61	1.08	2.66	1.09	2.66	1.18	2.73	1.26
4.00	2.56	0.99	2.59	1.08	2.65	1.09	2.68	1.18	2.78	1.20
3.90	2.54	1.02	2.59	1.09	2.66	1.10	2.72	1.17	2.77	1.13
3.80	2.54	1.05	2.61	1.10	2.69	1.09	2.74	1.12	2.74	1.11
3.70	2.58	1.08	2.64	1.08	2.70	1.06	2.72	1.09	2.71	1.12
3.60	2.64	1.06	2.65	1.05	2.70	1.03	2.70	1.09	2.71	1.16
3.50	2.64	1.03	2.64	1.04	2.68	1.04	2.69	1.13	2.77	1.22
3.40	2.63	1.02	2.63	1.05	2.69	1.06	2.73	1.18	2.85	1.27
3.30	2.63	1.06	2.65	1.10	2.73	1.10	2.81	1.22	3.00	1.29
3.20	2.67	1.11	2.70	1.13	2.80	1.13	2.94	1.23	3.18	1.20
3.10	2.74	1.15	2.79	1.16	2.91	1.13	3.10	1.17	3.31	1.02
3.00	2.86	1.18	2.92	1.14	3.04	1.06	3.21	1.01	3.30	0.84
2.90	3.03	1.12	3.05	1.04	3.12	0.94	3.22	0.85	3.27	0.71
2.80	3.14	0.96	3.10	0.91	3.14	0.80	3.19	0.73	3.22	0.62
2.70	3.14	0.80	3.10	0.79	3.12	0.70	3.15	0.64	3.18	0.55
2.60	3.11	0.71	3.07	0.71	3.09	0.62	3.11	0.58	3.14	0.50
2.50	3.08	0.64	3.05	0.64	3.05	0.57	3.07	0.53	3.11	0.46
2.40	3.05	0.58	3.03	0.59	3.03	0.52	3.04	0.50	3.08	0.42
2.30	3.02	0.54	3.01	0.55	3.00	0.49	3.02	0.47	3.06	0.39
2.20	3.00	0.51	2.99	0.52	2.98	0.46	3.01	0.44	3.05	0.36
2.10	2.99	0.48	2.98	0.49	2.97	0.43	2.99	0.42	3.04	0.34
2.00	2.98	0.46	2.97	0.47	2.96	0.41	2.98	0.39	3.04	0.31
1.95	2.97	0.45	2.97	0.45	2.96	0.40	2.98	0.38	3.05	0.28
1.90	2.97	0.43	2.97	0.44	2.96	0.39	2.98	0.37	3.04	0.24
1.85	2.96	0.42	2.96	0.43	2.95	0.38	2.99	0.36	3.02	0.23
1.80	2.96	0.41	2.97	0.42	2.96	0.37	2.99	0.35	3.03	0.22
1.75	2.96	0.40	2.97	0.40	2.96	0.35	3.00	0.33	3.04	0.18
1.70	2.96	0.39	2.97	0.39	2.96	0.34	3.01	0.31	3.03	0.14
1.65	2.96	0.38	2.97	0.38	2.97	0.33	3.01	0.28	2.99	0.08
1.60	2.96	0.37	2.98	0.37	2.97	0.31	3.00	0.26	2.94	0.07
1.55	2.97	0.36	2.98	0.36	2.98	0.29	3.00	0.24	2.92	0.07
1.50	2.97	0.35	3.00	0.34	2.99	0.27	3.02	0.22	2.89	0.06
1.45	2.98	0.34	3.01	0.32	2.98	0.24	3.04	0.16	2.87	0.06
1.40	2.99	0.33	3.02	0.28	2.98	0.22	2.99	0.11	2.86	0.06
1.35	3.00	0.32	3.01	0.26	3.00	0.20	2.99	0.09	2.84	0.05
1.30	3.01	0.30	3.02	0.24	3.01	0.15	2.94	0.04	2.83	0.05
1.25	3.03	0.27	3.03	0.21	2.98	0.09	2.90	0.04	2.82	0.05
1.20	3.02	0.24	3.05	0.15	2.94	0.06	2.87	0.04	2.80	0.04
1.15	3.02	0.22	3.01	0.08	2.90	0.05	2.85	0.04	2.79	0.04
1.10	3.03	0.21	2.96	0.06	2.87	0.05	2.83	0.03	2.78	0.04
1.05	3.07	0.18	2.92	0.05	2.85	0.04	2.82	0.03	2.77	0.04
1.00	3.05	0.05	2.90	0.05	2.84	0.04	2.81	0.03	2.77	0.03
0.95	2.98	0.04	2.88	0.05	2.82	0.04	2.79	0.03	2.76	0.03
0.90	2.95	0.04	2.86	0.04	2.81	0.03	2.78	0.03	2.75	0.03
0.85	2.92	0.04	2.85	0.04	2.80	0.03	2.77	0.02	2.74	0.03
0.80	2.90	0.04	2.84	0.04	2.79	0.03	2.76	0.02	2.74	0.03
0.75	2.89	0.03	2.83	0.03	2.78	0.03	2.76	0.02	2.73	0.02

shows interference fringes similar to those in the Ψ and Δ spectra, which are due to thickness nonuniformity in the film. The depolarization spectrum is modeled with 3.5% nonuniformity in the $CuIn_{0.69}Ga_{0.31}Se_2$ film thickness. Experimental data in the transparent region were analyzed with extra caution in order to separate critical points $E_0(A)$, $E_0(B)$ and $E_0(C)$ from interference fringes. Further detailed descriptions of the fit strategies are beyond the scope of this article.

Figure 7 shows the second derivatives of the ε_2 spectrum for the $CuInSe_2$ film and the ordinary component of the $CuInSe_2$ single crystal (ε_2) spectrum generated from n and k values in Ref. 6. The CP energies in the ε_2 second derivative spectrum of the $CuInSe_2$ film match those of the $CuInSe_2$ crystal. $E_0(A)$ and $E_0(B)$ are not resolved in either spectrum so the first transitions are marked $E_0(A,B)$. At the same time, the spin–orbit splitting is well resolved and the value

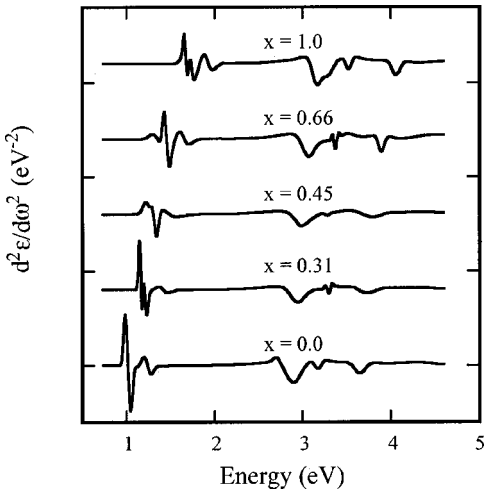

FIG. 9. Second derivative of the ε_2 spectra of $CuIn_{1-x}Ga_xSe_2$ films with varying Ga contents. All electronic transitions shift towards higher energy with an increase in Ga content.

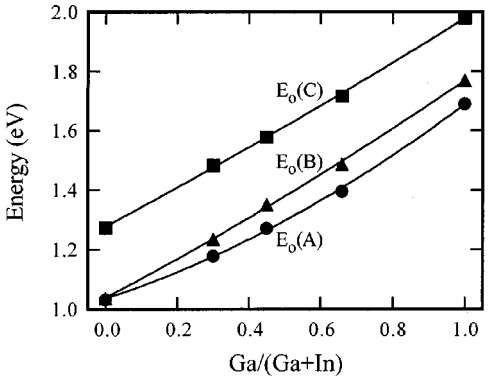

FIG. 10. Variation in fundamental absorption transitions $E_0(A)$, $E_0(B)$ and $E_0(C)$ of $CuIn_{1-x}Ga_xSe_2$ films with x.

Δ_{so} is 0.23 eV, consistent with the value reported for a bulk $CuInSe_2$ crystal.[29] Higher energy interband transitions corresponding to electronic transitions $E_1(A)$ and $E_1(B)$ at position N in the BZ and $E(\Delta X)$ at position T in the BZ are also visible and are shown in Fig. 7. In general, the good correlation between the film and crystal CP energies confirms the integrity of the optical model used in this analysis.

Figures 8(a) and 8(b) show optical constants n and k of $CuIn_{1-x}Ga_xSe_2$ films with $0 \leqslant x \leqslant 1$. Tabulated n and k values are listed in Table IV. The n and k values are provided in 50 meV intervals over the range of 0.75–2 eV to resolve the spin–orbit splitting, and in 100 meV intervals of 2–4.6 eV. In general, ellipsometry measurements are less sensitive to k values below the absorption band and published single crystal optical data are not readily available for comparison in this range. All electronic transitions shift towards higher energy with an increase in Ga content. The spin–orbit splitting is clearly visible in the n and k spectra for the entire Ga range in the films. The crystal field splitting is not distinguishable in the optical function spectra but can be clearly seen in the second derivative of the ε_2 spectra, which are shown in Fig. 9. CP energies obtained from the minima in the second derivative of the ε_2 spectra are listed in Table V. In general, the CP energies obtained are consistent with the oscillator energies shown in Table III. The crystal field splitting is not resolved in the $CuInSe_2$ films but becomes better resolved with increasing Ga concentrations. This can be explained by the fact that the distortion from cubic symmetry for $CuInSe_2$ is small compared to that for $CuGaSe_2$ so the crystal field is not large enough to resolve the peaks at room temperature. High-resolution electroreflectance measurements on $CuInSe_2$ gave $\Delta_{so}=0.233$ eV and $\Delta_{cf}=0.006$ eV at 77 K.[29] Figure 10 shows the variation in $E_0(A)$, $E_0(B)$ and $E_0(C)$ with the Ga concentration and can be fit with a second degree polynomial as shown in Eqs. (8)–(10). $E_0(A)$ for $CuInSe_2$ was determined using the electroreflectance result for Δ_{cf} from the literature.

$$E_0(A)=1.035+0.389x+0.264x^2, \tag{8}$$

$$E_0(B)=1.037+0626x+0.104x^2, \tag{9}$$

$$E_0(C)=1.276+0.644x+0.057x^2. \tag{10}$$

Since we assigned $E_0(A)$ to the lowest energy level according to convention, there is no crossover between energy levels $E_0(A)$ and $E_0(B)$ as one would expect from the crossover between valence bands Γ_{7v}^4 and Γ_{6v}^5 due to changes in the crystal field. As Eq. (8) shows, the optical bowing parameter for the fundamental band gap is 0.264, which is slightly higher than the bowing parameter of 0.21 based on a theoretical calculation for stoichiometric material.[3] However, the results based on experiments were largely scattered[3] and varied from 0.11 (Ref. 30) to 0.24 (Ref. 31) for evaporated films. This large discrepancy in the bowing parameter could be partly due to the deviation in Cu stoichiometry.[22]

The spin–orbit splitting and crystal field splitting were determined using Eqs. (4) and (5) and are shown in Fig. 11. The ordering of valance bands Γ_{7v}^4 and Γ_{6v}^5 was determined from the crystal data for similar compositions reported in the literature.[4] The error bars shown are the SE measurement resolution due to the energy step used for this study. The Δ_{so} shows upward bowing and the values are consistent with other results reported in the literature.[4,32] Small differences in the data could be due to stoichiometric deviations in the samples. The negative values for Δ_{cf} are in accordance with the polarization selection rule and negative crystal field observed in $CuIn_{1-x}Ga_xSe_2$ ternary chalcopyrites.[4,33,34] The crystal field splitting shows a nonlinear dependence with the Ga concentration. Vegard's law suggests a linear variation in the c/a ratio according to Ga content, which results in a linear variation in the crystal field splitting based on the

TABLE V. Variation in the electronic transition energies with the Ga/(Ga + In) ratio obtained from Fig. 9.

Ga/(Ga+In)	$E_0(A)$ (eV)	$E_0(B)$ (eV)	$E_0(C)$ (eV)	$E_1(A)$ (eV)	$E(X\Gamma)$ (eV)	$E_1(B)$ (eV)
0.00		1.03	1.27	2.91	3.19	3.66
0.31	1.18	1.23	1.48	2.96	3.31	3.74
0.45	1.27	1.35	1.58	3.02	3.34	3.84
0.66	1.40	1.49	1.72	3.07	3.37	3.91
1.00	1.69	1.77	1.98	3.17	3.52	4.06

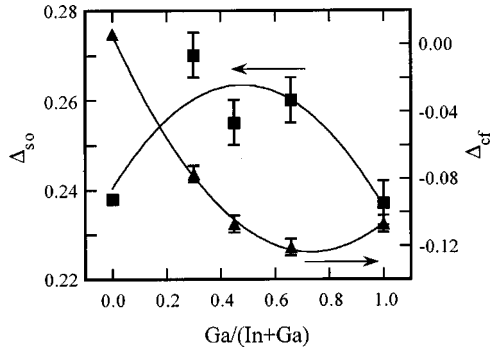

FIG. 11. Variation in the Δ_{cf} and Δ_{so} of $CuIn_{1-x}Ga_xSe_2$ films with x. The nonlinear behavior of the crystal field splitting could be due to the effect of anion displacement.

compression rule described in Eq. (2). However, the nonlinear behavior observed in the data may be caused by the fact that for Cu-based ternary chalcopyrites the crystal field splitting is not purely dependent on the tetragonal distortion.[2] Band structure calculations show that the optical band gap is also influenced by anion displacement.[34] The accuracy of crystal field splitting data is limited by the nature of the sample: they are slightly textured polycrystalline films. For more accurate values, measurements on single crystal or epitaxial films are recommended.

Higher interband transitions are also visible in the ε_2 spectra. Figure 12 shows the effect of Ga variation on transitions $E_1(A)$, $E(X\Gamma)$ and $E_1(B)$. $E(X\Gamma)$ corresponds to the transition at the BZ center from $\Gamma_{5v}^{(2)}$ to Γ_{1c}. $E_1(A)$ and $E_1(B)$ correspond to transitions at edge point N in the BZ. $E(\Delta X)$, which corresponds to an electronic transition at T in the BZ, is not clearly visible for all compositions.

V. CONCLUSIONS

The surface roughness of polycrystalline $CuIn_{1-x}Ga_xSe_2$ films deposited by four-source coevaporation made them unsuitable for SE analysis. A method was developed to circumvent this problem by performing the SE measurement on the reverse side of the films after they were peeled from the substrate. The films peeled cleanly from the substrate, probably due to the presence of $MoSe_2$, and smooth crack-free $CuIn_{1-x}Ga_xSe_2$ films were obtained. The presence of an optically thick Mo film, deposited prior to the peeling, made the optical modeling easier. Also, the rms roughness from AFM measurements performed after Mo deposition provided an estimate of the interface layer thickness.

A detailed description of the SE measurement and multilayer modeling strategy generic to ternary chalcopyrite semiconductors was presented. The optical functions obtained were compared with the data reported in the literature for single/polycrystalline ingots. The optical constants measured on polycrystalline $CuIn_{1-x}Ga_xSe_2$ films were found to be similar to the ordinary component of the single crystal optical constants. A comparison of the ε_2 spectra of a $CuInSe_2$ film and of a single crystal shows that the polycrystalline nature of the film did not affect the optical constants. This indicates that the change in path length as a result of grain boundary reflection is not significant for these films. In other words, the evaporated $CuIn_{1-x}Ga_xSe_2$ films are compact and large grained. SE measurements in anisotropy mode show that the deviation from random orientation did not cause any measurable anisotropy in the film.

The effect of the Ga concentration on different optical transitions in the dielectric spectra was shown in detail. As the Ga concentration increases, the electronic transitions shift towards higher energies, consistent with the theoretical and experimental results reported in the literature. $CuIn_{1-x}Ga_xSe_2$ thin films show a triply degenerate fundamental transition consistent with the chalcopyrite band structure. The degeneracy was removed by crystal field splitting and spin–orbit interaction. $CuIn_{1-x}Ga_xSe_2$ films show negative crystal field splitting. For $CuInSe_2$ the crystal field splitting is negligibly small and is not measurable in room temperature SE measurements. As the Ga concentration increased, the crystal field splitting increased, similar to the results reported for polycrystalline ingots in the literature. Nonlinear behavior was observed, in contradiction to the linear behavior expected from Vegard's law and the compression rule. The reason for this nonlinear behavior could be anion displacement, a result of the two cations in the $CuIn_{1-x}Ga_xSe_2$ lattice. The bowing parameter for the band gap is slightly higher than the values reported in the literature based on theoretical calculation. Second order polynomial equations for the Ga dependence of the fundamental electronic transitions and tabulated values of optical constants were presented.

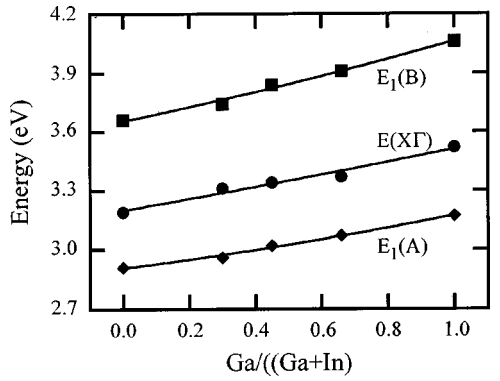

FIG. 12. Variation in the higher energy transitions of $CuIn_{1-x}Ga_xSe_2$ films with x.

ACKNOWLEDGMENTS

The authors thank M. Haimbodi, K. Hart and T. Hughes-Lampros for technical assistance. This work was supported in part by the National Renewable Energy Laboratory under Subcontract No. ADJ-1-30630-12.

[1] J. E. Jaffe and A. Zunger, Phys. Rev. B **28**, 5822 (1983).
[2] S. B. Zhang, S.-H. Wei, and A. Zunger, Phys. Rev. B **57**, 9642 (1998).
[3] S.-H. Wei and A. Zunger, J. Appl. Phys. **78**, 3846 (1995).
[4] M. I. Alonso, M. Garriga, C. A. Durante Rincón, E. Hernández, and M. León, Appl. Phys. A: Mater. Sci. Process. **A74**, 659 (2002).
[5] T. Kawashima, S. Adachi, H. Miyake, and K. Sugiyama, J. Appl. Phys. **84**, 5202 (1998).
[6] M. I. Alonso, K. Wakita, J. Pascual, M. Garriga, and N. Yamamoto, Phys. Rev. B **63**, 075203 (2001).

[7] A. M. Hermann *et al.*, Sol. Energy Mater. Sol. Cells **70**, 245 (2001).
[8] A. M. Hermann, C. Gonzalez, P. A. Ramakrishnan, D. Balzar, C. H. Marshall, J. N. Hilfiker, and T. Tiwald, Thin Solid Films **387**, 54 (2001).
[9] V. V. Kindyak, A. S. Kindyak, V. F. Gremenok, and I. A. Victorov, Thin Solid Films **293**, 75 (1997).
[10] P. Guha, S. N. Kundu, S. Chaudhuri, and A. K. Pal, Mater. Chem. Phys. **74**, 192 (2002).
[11] S. Shirakata, S. Chichibu, H. Miyake, and K. Sugiyama, J. Appl. Phys. **87**, 7294 (2000).
[12] W. N. Shafarman, R. Klenk, and B. E. McCandless, J. Appl. Phys. **79**, 7324 (1996).
[13] W. Shafarman and J. Zhu, Thin Solid Films **361–362**, 473 (2000).
[14] J. Hedström, H. Ohlsen, M. Bodegård, A. Kylner, L. Stolt, D. Hariskos, M. Ruckh, and H. Schock, *Proceedings of the 23rd IEEE PVSC* (IEEE, Piscataway, NJ, 1993), p. 364.
[15] J. A. Wollam, B. Johs, C. M. Herzinger, J. Hilfiker, R. Synowicki, and C. L. Bungay, Proc. SPIE **CR72**, 3 (1999).
[16] Guide to using WVASE32®, software for VASE, J. A. Woollam Co.
[17] S. Adachi, *Optical Properties of Crystalline and Amorphous Semiconductors* (Kluwer Academic, Boston, 1999), p. 63.
[18] D. Stroud, Phys. Rev. B **12**, 3368 (1975).
[19] M. I. Alonso, M. Garriga, C. A. Durante Rincón, and M. M. León, J. Appl. Phys. **88**, 5796 (2000).
[20] J. Camassel, L. Artus, and J. Pascual, Phys. Rev. B **41**, 5717 (1990).
[21] B. Tell and P. M. Bridenbaugh, Phys. Rev. B **12**, 3330 (1975).
[22] S. Chichibu, T. Mizutani, K. Murakami, T. Kurafuji, H. Nakanishi, S. Niki, P. J. Fons, and A. Yamada, J. Appl. Phys. **83**, 3678 (1998).
[23] J. J. Hopfield, J. Phys. Chem. Solids **15**, 97 (1960).
[24] C. M. Herzinger and B. Johs, U. S. Patent No. 5,796,983 (filed 14 August 1995, issued 18 August 1998).
[25] D. W. Marquardt, J. Soc. Ind. Appl. Math. **11**, 431 (1963).
[26] G. B. Harris, Philos. Mag. **43**, 113 (1952).
[27] G. E. Jellison, Jr., Thin Solid Films **313–314**, 33 (1998).
[28] T. Holden, P. Ram, F. H. Pollak, J. L. Freeouf, B. X. Yang, and M. C. Tamargo, Phys. Rev. B **56**, 4037 (1997).
[29] H. Newman, Sol. Cells **16**, 317 (1986).
[30] B. Dimmler, H. Dittrich, R. Menner, and H. W. Schock, *Proceedings of the 19th IEEE PVSC* (IEEE, Piscataway, NJ, 1993), p. 1454.
[31] D. S. Albin, J. J. Carapella, J. R. Tuttle, and R. Noufi, Mater. Res. Soc. Symp. Proc. **228**, 267 (1991).
[32] C. A. Durante Rincón, E. Hernández, M. I. Alonso, M. Garriga, S. M. Wasim, C. Rincón, and M. León, Mater. Chem. Phys. **70**, 300 (2001).
[33] J. L. Shay, E. Buehler, and J. H. Wernick, Phys. Rev. Lett. **24**, 1301 (1970).
[34] J. E. Jaffe and A. Zunger, Phys. Rev. B **27**, 5176 (1983).